NONLINEAR DYNAMIC SOIL-PILE-STRUCTURE-INTERACTION ANALYSIS OF OFFSHORE PLATFORM FOR DUCTILITY LEVEL EARTHQUAKE UNDER SOIL LIQUEFACTION CONDITIONS

Bor-Feng Peng[1], Ben Chang[2], Bee-Lay Leow[3] and Sam Nandlal[4]

[1] *Principal Engineer, PE, Ph.D.,* [2] *Senior Staff Consultant, PE, Ph.D., F.ASCE,* [3] *Principal Engineer, Dept. of Structural Engineering, J. Ray McDermott Engineering, LLC, Houston. Texas, USA*

[4] *Structural Engineer, PE, Ph.D., BG Trinidad & Tobago Limited, Port of Spain, Trinidad & Tobago*

Email: bfpeng@mcdermott.com, sschang@mcdermott.com, blleow@mcdermott.com, sam.nandlal@bg-group.com

ABSTRACT:

This paper presents the rigorous methodology and structural analysis procedures required for nonlinear dynamic soil-pile-structure-interaction analysis of offshore platforms under ductility level earthquakes with emphasis on the soil liquefaction conditions. The nonlinear inelastic soil properties including the cyclic strain rate, gapping, and the hysteretic energy dissipation are considered. The non-linear beam-column element and non-linear strut element, which were calibrated with numerous test results for offshore structures, are modeled and presented. Three sets of representative ground motion time histories, which characterize the likely envelop of ground intensity, frequency content, phasing and duration expected at the site, are considered in the analysis. The comparison of the evolutionary power spectral density of the earthquake ground motion accelerations is outlined for soil liquefaction and non-liquefaction conditions in terms of the intensity and frequency content of the ground motion accelerations. The impact of the soil liquefaction conditions on the structural response and especially for the pile foundation system design, are illustrated using a recently successfully designed platform in the seismic active area offshore Trinidad. API and ISO seismic design requirements are briefly discussed. The most critical structural components of the pile-jacket connections design are demonstrated by the nonlinear finite element analysis with the large deformation of the platform and the material plasticity of the steel considered.

KEYWORDS: soil liquefaction, evolutionary power spectral density, offshore platform, ductility level earthquake, soil-pile-structure interaction

INTRODUCTION

With the ever increasing world energy demand, the design of offshore structures under severe environmental conditions has become more essential, critical, and challenging. Recently, more offshore platforms are designed at locations subjected to rare and severe strong ductility level earthquake. If the first sand layer below mudline is too close to seabed, the sand layer could be liquefied due to high surface ground acceleration and excess pore water pressure developed in the sand layer during the strong earthquake. In order to prove the offshore platform is stable without structure collapse, the nonlinear soil-pile-structure interaction time histories analysis is recommended by API RP 2A and ISO 19902 to demonstrate the platform structure-foundation system meets structural reserve strength and energy dissipation requirements. Per API RP 2A, at least three set of representative ground motion time histories should be analyzed to demonstrate that the structure-foundation system remains stable under the loads imposed by these ground motions. In ISO 19902 seismic design procedures and criteria, the structure-foundation response shall be determined to at least four sets of ground-motions records characterizing the likely intensity, frequency content, and duration of DLE event. If less than 7 sets of time history records are used, the objective may be considered met if at least four sets of earthquake records do not cause platform collapse. If seven or more sets of earthquake records are used, more than half should not cause collapse. The API RP 2A analysis procedures are followed and presented in this paper with emphasis on the impact of soil liquefaction conditions on the platform dynamic response and foundation system design. The soil liquefaction assessment requirements and procedures are outlined with assessment results presented. The time histories simulation method and parameters of earthquake ground motions are illustrated with simulated time histories and the corresponding evolutionary power spectral density.

PLATFORM STRUCTURAL ANALYSIS MODEL

The platform model shown in Figure 1 includes the topsides, jacket, foundation piles and nonlinear soil elements. Using offshore structure analysis software MicroSAS II, the space frame model includes all the important characteristics of the stiffness, mass, energy dissipation, marine growth and loading properties of the structure and foundation components. The analytical model consists primarily of tubular and I-shaped beam elements. The design topsides payload is about 19976 kips and the jacket mass is about 19018 kips. The topsides mainly consist of drilling deck, production deck, mezzanine deck, and cellar deck. The jacket primary frames include the vertical and launch truss frames and seven main horizontal frames. The water depth is about 530 feet. The jacket is 553 ft long and battered from 180 ft x 180 ft near mud-line to 110 ft x 45 ft at EL (+) 18 ft. Appurtenances such as conductors, boat-landings, J-tubes, mud-mat frames, risers and casings are explicitly modeled. Under the in-service conditions, the non-structural items such as launch cradles, anodes, top of jacket walkways, mud-mats attachments, conductor guides, etc., are included solely to distribute load to the main members. These items are modeled as wave load objects and appurtenance masses. The casings, caissons, pull tubes, and the main legs below EL (-) 145 feet are flooded.

Foundation System

The foundation system includes twelve skirt-piles, nonlinear soil spring shown in Figure 2 and dash-pot elements. The leg and pile connections consist of the yoke plates, shear plates, skirt-pile sleeves, and grout connections. The lateral soil resistance is modeled by a set of orthogonal nonlinear springs normal to the axis of piles and having a nonlinear behavior described by "P-Y" curves. The resistance of the soil to pile penetration is modeled by nonlinear springs paralleled to the axis of the pile and having nonlinear behavior described by "T-Z" curves. The end-bearing is modeled by a no-tension spring located at the tip of the pile and acting along the axis of pile. The pile penetration is 370 feet.

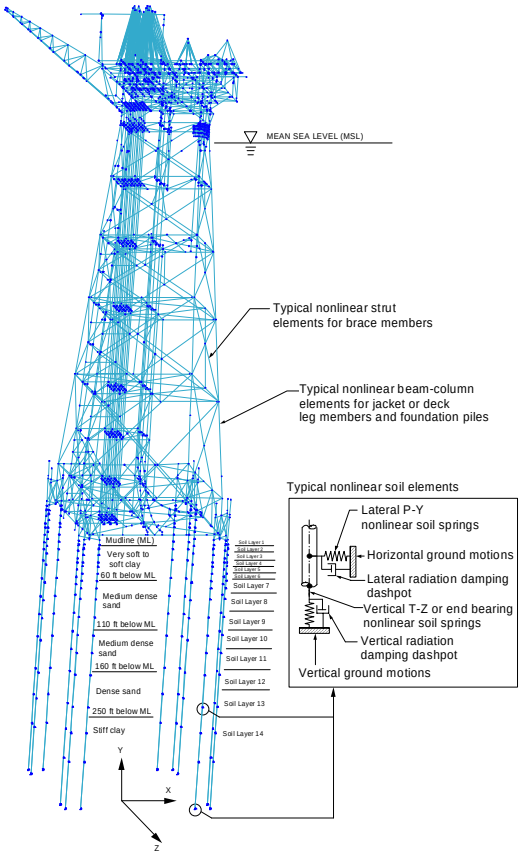

Figure 1 Platform structural analysis model

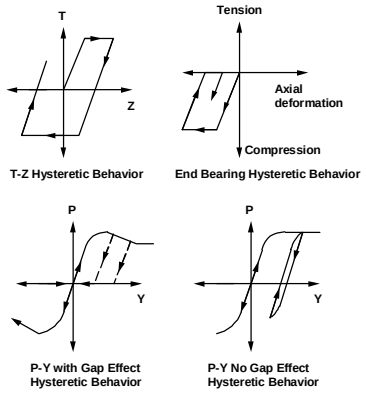

Figure 2 Hysteretic behavior of soil spring element

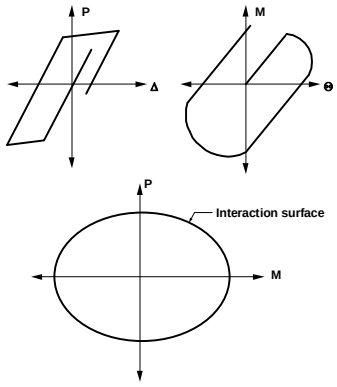

Figure 3 Nonlinear hysteretic behavior and yielding surface of the beam-column element

Nonlinear Beam-column Element and Strut Element

A nonlinear beam-column element is used to model the jacket legs, deck legs and skirt-piles. The nonlinear beam-column element will develop a plastic hinge at a particular end when the yield criterion defined by a specific yield surface is reached. The interaction surface for a tubular cross-section is represented by the equation $p_x^2 + m_y^2 + m_z^2 = 1.0$, where $p_x = P_x / P_u$, $m_y = M_y / M_{yp}$, and $m_z = M_z / M_{zp}$. The variable P_x is the axial force, P_u is the tension yield force or the ultimate buckling force of the element; M_y and M_z are the y-axis and z-axis moments, and the M_{yp} and M_{zp} are the y-axis and z-axis plastic bending moments. The typical hysteretic behavior and the yield surface of the beam-column element are displayed in Figure 3.

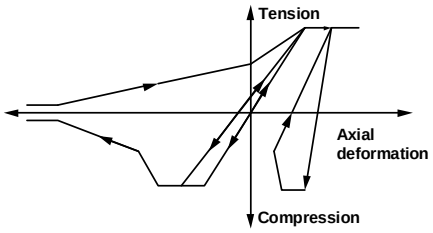

Figure 4 Nonlinear hysteretic behavior of strut element

The nonlinear brace strut element had been developed to model the tubular brace member and calibrated with numerous test results (API RP 2A-WSD). There are Marshall strut model, INTRA strut model, and Maison strut model. The strut element model in MicroSAS II adopts the INTRA strut element with modification to consider the Maison strut element behavior. The typical nonlinear load-displacement hysteretic property of the strut element is shown in Figure 4 including linear elastic, inelastic buckling under compressive load, and inelastic straightening under tensile load

SOIL LIQUEFACTION ASSESSMENT

An assessment of the potential liquefaction had been carried out and investigated for the sand layer between 61 feet and 248 feet below sea-bed. The procedure of the liquefaction susceptibility assessment follows the NCEER recommended empirical approach described by Brandes (2003) and Youd & Idriss (2001). Calculation or estimation of two variables is required for evaluation of liquefaction resistance of soils: (1) the seismic demand on a soil layer, expressed in terms of cyclic stress ratio (CSR), and (2) the capacity of the soil to resist liquefaction, expressed in terms of cyclic resistance ratio (CRR). The cyclic stress ratio is formulated as $CSR = 0.65(a_{\max}/g)(\sigma_{vo}/\sigma'_{vo})r_d$, where $a_{\max}$ is the peak horizontal acceleration at the ground surface (mudline) during earthquake; g is the gravity acceleration; σ_{vo} and σ'_{vo} are total and effective overburden stresses, respectively; and r_d is the stress reduction coefficient which is function of soil depth. Note the stress due to the effect of the water above mudline is excluded since the total stress in this calculation represents inertia effects in the soil, not the water above it. For clean-sand, the CRR can be approximately expressed as:

$$CRR = 1/[34 - (N_1)_{60}] + (N_1)_{60}/135 + 50/[10 \cdot (N_1)_{60} + 45]^2 - 1/200 \quad (1)$$

The corrected SPT blow count $(N_1)_{60}$ is calculated from the measured blow count N_m using the equation as $(N_1)_{60} = N_m C_N C_E C_B C_R C_S$, where C_N is the correction factor for overburden stress and is commonly calculated as $\sqrt{P_a / \sigma'_{vo}}$ in which P_a represents the atmospheric pressure of approximate 96 kPa; C_E is a correction factor for SPT hammer energy and defined as ER/60 (ER is the energy ratio transferred from hammer to SPT sampler); C_B is a correction factor for borehole diameter; C_R is a correction factor for rod length; and C_S is a correction factor for sampling method with or without liners. For sand with fines content greater than 5%, the equivalent clean sand value $(N_1)_{60cs}$ is evaluated approximately by the equations: $(N_1)_{60cs} = \alpha + \beta \cdot (N_1)_{60}$, where α and β are determined based on the fines content (FC) of the sand and expressed as: $\alpha = 0, \beta = 1$, for FC $\leq$ 5%; $\alpha = 5, \beta = 1.2$, for FC $\geq$ 35%; and for 5% < FC < 35%, $\alpha = \exp[1.76 - (190/FC^2)]$, $\beta = 0.99 + (FC^{1.5}/1000)$. The last step is to plot the results on empirical liquefaction assessment chart in Figure 5. It is suggested that liquefaction may occur for the sand layer with depth 61 feet to 90 feet below seabed for a magnitude 7.5 ductility level earthquake with peak horizontal ground acceleration > 0.2G.

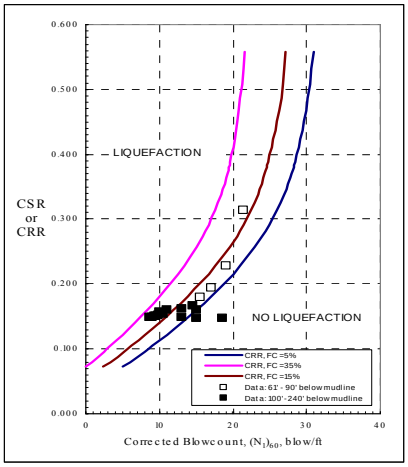

Figure 5 Liquefaction assessment chart based on STP data for magnitude 7.5 earthquake with peak horizontal ground acceleration = 0.2G

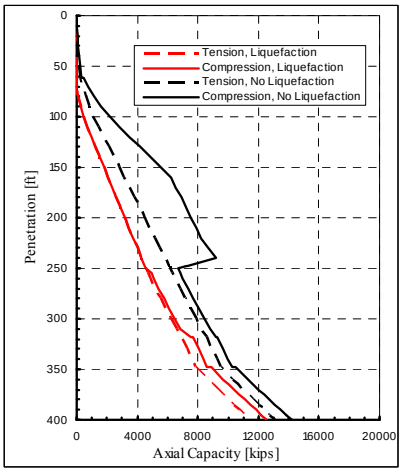

Figure 6 Ultimate Axial Capacity [kips] 84-in Diameter Pile (2134-mm)

IMPACT OF SOIL LIQUEFACTION ON SHEAR STRENGTH AND AXIAL PILE CAPACITY

The residual shear strength or the liquefied shear strength $S_u(LIQ)$ is evaluated according to the liquefied strength ratio approach of Olson and Stark (2002) to determine the reduced axial pile capacity, p-y and t-z curves due to liquefied sand layer. The liquefied strength ratio $S_u(LIQ)/\sigma'_{vo}$ is defined as the liquefied residual shear strength normalized by the pre-liquefied or pre-failure vertical effective stress. The average trend-lines are described as: $S_u(LIQ)/\sigma'_{vo} = 0.03 + 0.0075\left[(N_1)_{60}\right] \pm 0.03$ for $(N_1)_{60} \le 12$ (2)

Figure 6 shows the comparison of the 84"Ø pile ultimate axial capacity under non-liquefied and liquefied soil conditions. It is noted that the reduction of the pile ultimate axial capacity is dependent of the pile penetration depth. For penetration depth of 200 ft, the reduction of pile axial ultimate compression capacity is more than 50% while pile axial ultimate compression capacity is reduced by only 7% for deeper penetration (e.g., 370 ft).

GROUND MOTION TIME HISTORIES

The three sets of ground accelerations based on seismic hazard analysis are developed by URS using the ProShake code. This code was calibrated previously against motions recorded at the Wildlife, California, and Port Island, Japan, sites, which liquefied during 1986 Superstition Hills and 1995 Kobe earthquake, respectively. The ground acceleration time histories are generated for both liquefaction and non-liquefaction cases at the following depth (ft) below mud-line: 0, 10, 20, 30, 40, 50, 60, 85, 110, 135, 160, 190, 220, and 250. Both horizontal components from three accelerograms recorded during representative earthquakes were selected and modified to be compatible with the level of 2000-year return period response spectrum. The earthquake outcrop motions are generated at the top of the medium-dense sand layer (110-ft depth). Pertinent information of these accelerograms is provided in Table 1. The site response analysis was not conducted for the vertical component since the variation in the soil vertical motion with depth is not significant per experiences. Therefore, the vertical-component of the outcrop motions is used at all the soil layers. The soil layers consisted of very soft to soft clay, medium-dense to dense sand, and stiff clay. The simulated shear-wave velocity (V_s) and associated soil layers are summarized in Table 2. More detailed information can be found in the seismic hazard analysis report by URS in the references. Note that modeling the liquefied sand as a linear viscoelastic material with a shear wave velocity of 66 ft/s and a material damping ratio of 20%, yielded motions (from SHAKE analysis) that were in reasonable agreement with the recorded ground motions. Typical Plots of these simulated records are presented in Figures 7 and 8. It is worthy to note that the ground motion intensity has been significantly reduced due to the liquefied sand layer near the ground surface. The liquefied sand layer effectively acts as a "base-isolator" which filters the short and intermediate period ground motions and shifts the response of soil column with longer periods. To illustrate the time variation of frequency content and

intensity of the ground motions, the evolutionary or time-varying power spectral density (TPSD) of ground acceleration time histories is displayed in the Figures 9 and 10 to illustrate the impact of liquefied soil sand layer on the characteristics of ground motions. The TPSD is estimated by short-time Thomson's multiple-window spectrum estimation (Conte & Peng, 1997).

Table 1 Representative records for ProShake analysis

Earthquake			Record	
Year	Name	M	Station	Components
1940	Imperial Valley (CA, USA)	7.1	El Centro	180˚ and 270˚
1978	Tabas (Iran)	7.4	Dayhook	190˚ and 280˚
1992	Landers (CA, USA)	7.3	Yermo	Fault-Normal and Fault-Parallel

Table 2 Soil layer properties and V_s

Soil Depth (ft) below Mudline	Description	Low Strain V_s (ft/s)
0 ~ 60	Very soft to soft clay	250 ~ 550
60 ~ 110	Medium dense sand	550 ~ 650 (non-liquefied) or 66 (liquefied)
110 ~ 160	Medium dense sand	750
160 ~ 250	Dense sand	850
> 250	Stiff Clay	850

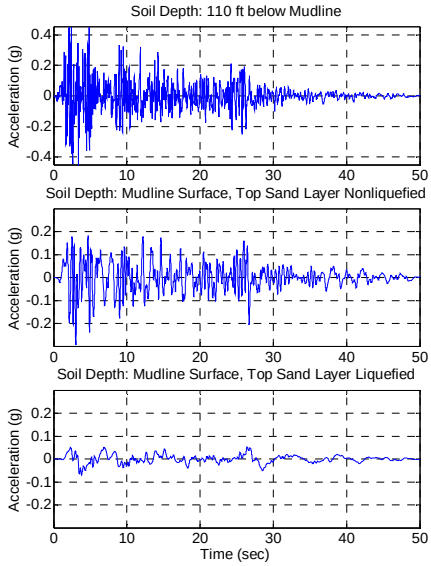

Figure 7 Modified 1940 El Centro records, 180˚ horizontal component

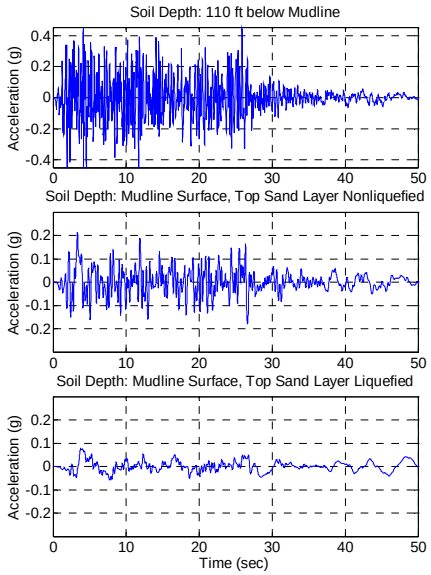

Figure 8 Modified 1940 El Centro records, 270˚ horizontal component

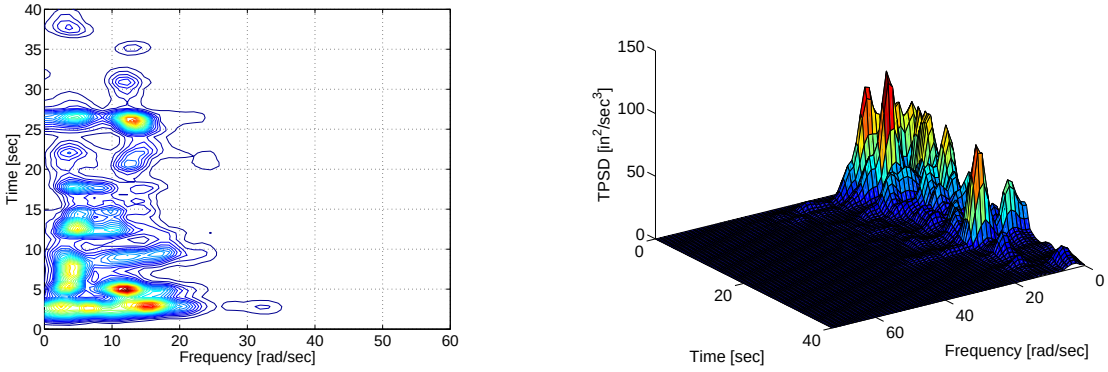

Figure 9 TPSD and contour plot of ground acceleration (180˚ horizontal component) at mudline, modified 1940 El Centro earthquake with top sand layer non-liquefied

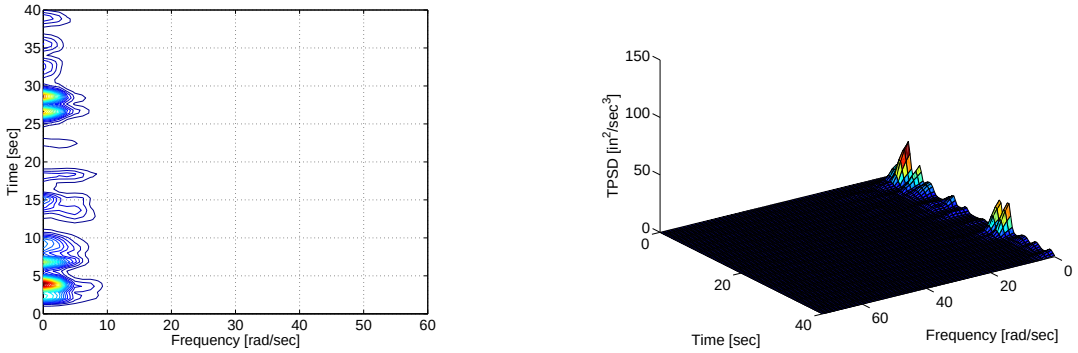

Figure 10 TPSD and contour plot of ground acceleration (180° horizontal component) at mudline, modified 1940 El Centro earthquake with top sand layer liquefied

IMPACT OF SOIL LIQUEFACTION ON PLATFORM RESPONSE AND PILE DESIGN

Nonlinear Structural Element Behavior

The typical nonlinear structural element response of the topsides and the jacket are illustrated in Figures 11 and 12. It is found that the topsides and jacket are subjected to more members with nonlinear behavior for non-liquefied soil condition. However, the number of members developing nonlinear structural response under modified El Centro earthquake with liquefied soil condition has been significantly reduced. This can be explained by the reduced intensity of the ground surface accelerations shown in Figure 7 through Figure 10 due to liquefied soil. The platform-foundation system become softer with natural period increased and the platform dynamic amplification will be reduced as seen in the typical response spectra in design codes. It is noted that the base torsional moment is always about 70% higher for soil non-liquefied condition than that for liquefied case. This is one of the primary causes to trigger more members developing nonlinear hysteretic behavior.

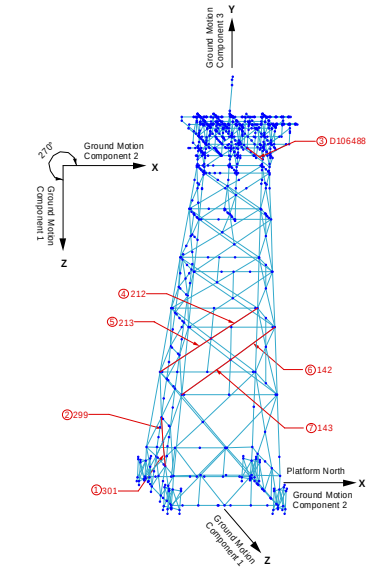

Sequence and the nonlinear behavior of damaged members			
Event	Time (sec)	Member	Nonlinear Behavior
1	2.350	301	buckling plateau
2	2.360	299	buckling plateau
3	4.360	D106488	buckling plateau
4	5.260	212	post-buck env1
5	5.270	213	buckling plateau
6	7.800	142	buckling plateau
7	7.800	143	buckling plateau

Figure 11 Modified El Centro earthquake, heading angle θ = 270° without sand layer liquefied

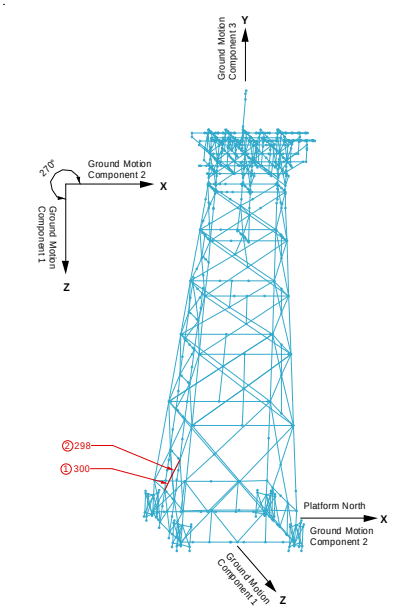

Sequence and the nonlinear behavior of damaged members			
Event	Time (sec)	Member	Nonlinear Behavior
1	2.940	300	BUCKLING PLATEAU
2	2.950	298	BUCKLING PLATEAU

Figure 12 Modified El Centro earthquake, heading angle θ = 270° with sand layer liquefied

Pile and Pile to Jacket Leg Connection Design

Typical pile bending moment envelopes for liquefied or non-liquefied soil conditions under various simulated earthquakes are shown in Figure 13. It is found that the maximum bending moment is always located at soil depth about 110 feet below mudline (i.e., interface between liquefied and non-liquefied sand layers) for sand layer liquefied condition. Under modified El Centro and Dayhook earthquakes, the maximum bending moments of piles develop at relatively shallow location for non-liquefied soil condition. The wall thickness demand of the pile for liquefied soil condition is in general greater than that for non-liquefied case due to the larger bending moments of piles at the pile head or soil depth near 110 feet below mudline.

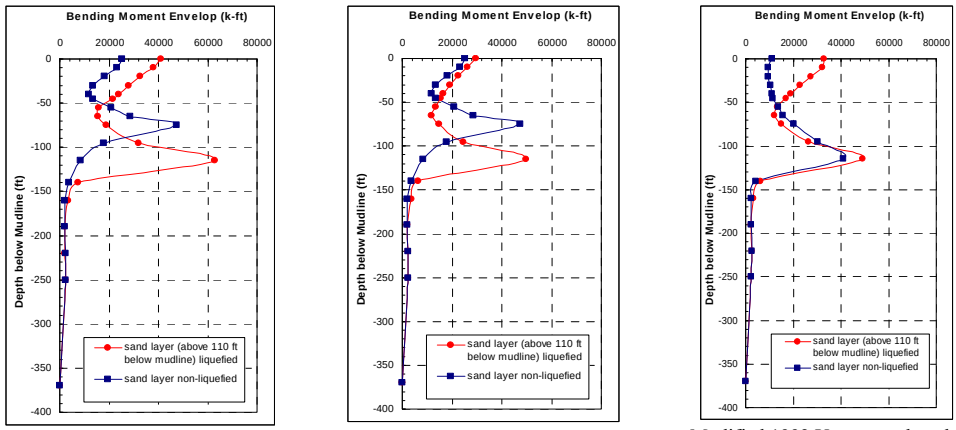

Modified 1940 El Cento earthquake Modified 1978 Dayhook earthquake Modified 1992 Yermo earthquake

Figure 13 Pile bending moment envelops for liquefied and non-liquefied soil conditions under various earthquakes

The nonlinear finite element analysis is performed for strength and buckling check of the most critical structural components of pile to jacket leg connection. The material plasticity of the steel plates with large deformation or nonlinear geometric effects is considered. From Figure 14, it is shown that high stresses are near the jacket leg connected to the top yoke plate for soil non-liquefied condition. The local steel yielding is expected due to significant stiffness and geometry change. However, for soil liquefied condition, local high stresses are found near the pile head due to the larger displacement and bending moments of pile head at mudline. It is shown that the connection is stable without collapse under ductility level earthquake.

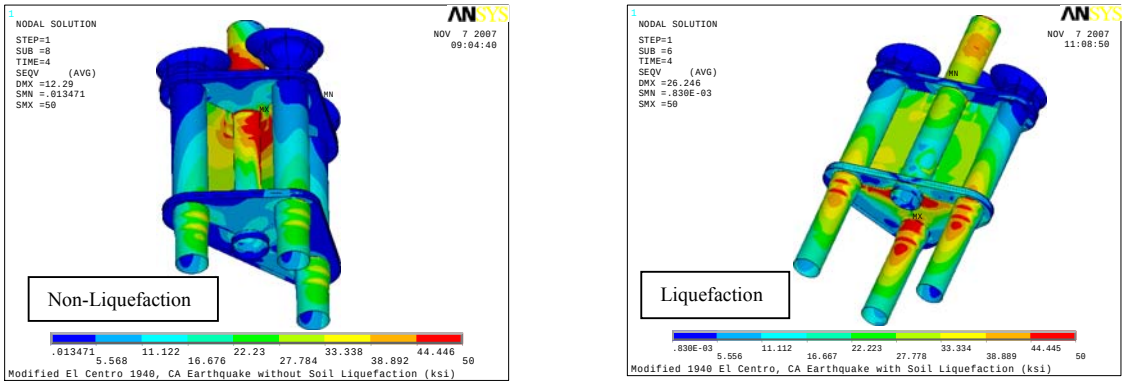

Figure 14 von Mises stress of pile to jacket leg connections

Topsides Dynamic Response and Pile-head Displacement

The most critical platform dynamic responses (i.e., the maximum displacements and the accelerations) of topsides are summarized in Table 3. It is shown that the maximum topsides displacements at drilling deck center could be increased by 100% for soil condition with liquefied sand layer in comparison with those for sand layers non-liquefied. The typical maximum pile-head lateral displacement at the mudline also increases significantly from about 7 inches to 17 inches due to the liquefied sand layer. The increase of the pile-head displacement had been cautiously examined to assess platform instability and P-Δ moments. The maximum

translational acceleration of the topsides at the center of drilling deck does not show any significant difference for soil conditions with liquefied or non-liquefied sand layer.

Table 3 Typical maximum displacements and translational accelerations at drilling deck center of topsides

Earthquake	θ (°)	Sand Layers Non-Liquefied			First Sand Layer below Mudline Liquefied		
		Maximum Topsides Displacement (inches)			Maximum Topsides Displacement (inches)		
		X-Direction	Y-Direction	Z-Direction	X-Direction	Y-Direction	Z-Direction
Modified 1940 El Centro	180	14.60	-4.64	16.99	28.44	-4.93	25.28
	225	16.84	-4.67	16.46	30.81	-4.96	33.41
		Maximum Topsides Acceleration (G)			Maximum Topsides Acceleration (G)		
		X-Direction	Y-Direction	X-Direction	Y-Direction	X-Direction	Y-Direction
Modified 1940 El Centro	180	0.69	0.61	0.54	0.65	0.69	0.58
	225	0.64	0.67	0.82	0.57	0.69	0.72

CONCLUSION

The rigorous methodology and required structural analysis procedures are presented for nonlinear dynamic soil-pile-structure-interaction analysis of offshore platforms under ductility level earthquakes with emphasis on the soil liquefaction conditions. The impact of soil liquefaction on the platform dynamic response and the foundation system design is significant and summarized as follows: (1) higher pile thickness demand; (2) deeper pile penetration depth requirement; (3) larger topsides and pile-head displacements; (4) longer periods of platform-foundation structural system; (5) reduced number of structural elements developing nonlinear hysteretic behavior if the platform is still stable; and (6) greater bending moment of pile developed at deeper depth. Based on nonlinear finite element analysis results of pile to jacket leg connection with material plasticity and larger deformation effects included and platform soil-pile-structure interaction analysis conclusions, this well-designed platform structure-foundation system would be stable and robust under rare intense ductility level earthquake even with the first sand layer below seabed liquefied.

ACKNOWLEDGEMENTS

The financial support from J. Ray McDermott Engineering (JRME), LLC, Houston Operation Center under the R & D Project No. 83150, is gratefully acknowledged. The writer would like to thank Richard Newhouse, Structural Department Manager of JRME, for review of this paper. Special thanks should be given to Phil Kageler for his coordination support of the structural design of the platform.

REFERENCES

American Petroleum Institute (2005). Recommended Practice for Planning Designing and Constructing Fixed Offshore Platform, API RP 2A-WDS, 21st Edition, Washington, DC, USA.

Brandes, H.G. (2003). Geotechnical and Foundation Aspects. Chapter 7 of Earthquake Engineering Handbook, edited by W-F Chen and C. Scawthorne, CRC Press.

Conte, J.P. and Peng, B-F. (1997). Fully nonstationary analytical earthquake ground-motion model. *Journal of Engineering Mechanics, ASCE,* **123:1,** 15-24.

International Standards Organization (2005). ISO 19902, Petroleum and Natural Gas Industries – Fixed Steel Offshore Structures.

Olson S.M. and Stark, T.D. (2002). Liquefied strength ratio from liquefaction flow failure case histories. *Canadian Geotechnical Journal,* **39,** 629-647.

Peng, B-F., Chang, B. and Llorente, C. (2005). Nonlinear dynamic soil-pile-structure interaction analysis of a deepwater platform for ductility level earthquake. *Proceedings of Offshore Technology Conference, Houston, TX, USA,* OTC paper **17274.**

URS Corporation (2007). Seismic Hazard Analysis and Development of Seismic Design Parameters for Poinsettia Offshore Platform Site in Trinidad, BG Trinidad & Tobago Limited.

Youd, T.L and Idriss, I.M. (2001). Liquefaction resistance of soils: summary report from the 1996 NCEER and 1998 NCEER/NSF workshops on evaluation of liquefaction resistance of soils. *Journal of Geotechnical and Geoenviromental Engineering, ASCE,* **127:4,** 297-313.